ACS APPLIED ENERGY MATERIALS

Article

Cite This: ACS Appl. Energy Mater. 2019, 2, 3131−3141

www.acsaem.org

Comparison of Pt−Cu/C with Benchmark Pt−Co/C: Metal Dissolution and Their Surface Interactions

Matija Gatalo,[†,‡] Primož Jovanovič,[*,▽] Urša Petek,[†] Martin Šala,[§] Vid Simon Šelih,[§] Francisco Ruiz-Zepeda,[†] Marjan Bele,[†] Nejc Hodnik,[▽] and Miran Gaberščček[*,†,‡]

[†]Department of Materials Chemistry, National Institute of Chemistry, Hajdrihova 19, 1000 Ljubljana, Slovenia

[‡]Faculty of Chemistry and Chemical Technology, University of Ljubljana, Večna pot 113, SI-1000 Ljubljana, Slovenia

[▽]Department of Catalysis and Chemical Reaction Engineering, National Institute of Chemistry, Hajdrihova 19, 1000 Ljubljana, Slovenia

[§]Department of Analytical Chemistry, National Institute of Chemistry, Hajdrihova 19, 1000 Ljubljana, Slovenia

S *Supporting Information*

ABSTRACT: Understanding of less-noble-metal (M) dissolution from Pt-alloy-based oxygen reduction reaction (ORR) electrocatalysts, as well its interaction with Pt surface, is crucial for maximizing their performance. In pursuing this goal, two ORR electrocatalysts—a benchmark Pt−Co/C and an in-house designed Pt−Cu/C materials—are investigated. Both are characterized with a range of standard techniques, such as X-ray diffraction (XRD), transmission electron microscopy (TEM) combined with energy dispersive spectroscopy (EDX) and thin film-rotating disc electrode (TF-RDE) measurements. A special focus is put on combining the latter with a highly sensitive electrochemical flow cell (EFC) online connected to inductively coupled plasma mass spectrometry (ICP-MS) measurements. A combination of standard and novel techniques provides unprecedented insights into the dissolution behavior and dynamics of metals, as well as their subsequent surface interactions and effects on the electrochemical performance. A special focus is devoted to the significance of electrocatalyst activation protocols and their effects on metal dissolution. Distinct differences in the behavior of Pt−Cu and Pt−Co alloys are revealed, which will help develop proper protocols for practical implementation of Pt-alloy electrocatalysts.

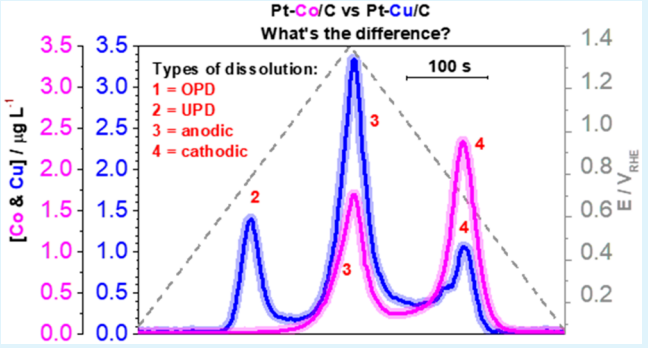

KEYWORDS: *oxygen reduction reaction, proton exchange membrane fuel cell, platinum alloy, metal dissolution, electrochemical flow cell coupled to inductively coupled plasma mass spectrometer*

INTRODUCTION

Being one of the cornerstones of the sustainable energy politics, hydrogen technology is believed to play an essential role in the near future. Especially low-temperature proton exchange membrane fuel cells (PEMFC), together with batteries, are expected to compete with and eventually replace conventional energy infrastructure.[1] In the recent years, two major challenges, such as high cost of Pt and sluggish kinetics of the cathode oxygen reduction reaction (ORR), have been successfully tackled,[2] bringing this technology on the doorstep of commercialization.[3] The progress is mainly attributed to the successful use of nanoparticulate Pt-based alloys (Pt−M) with less expensive 3d transition metals (M = Cu, Co, and Ni to mention the most common ones), which are currently considered as state-of-the-art ORR electrocatalysts. They not only enable better utilization of Pt atoms by wasting a lower number of core Pt atoms inside the nanoparticles[4] but can also substantially enhance ORR specific activity by the well-known ligand or strain effect.[5] This enables a decrease of the Pt loading without losses in the overall PEMFC performance and thus substantially reduces the cost. Along these lines, recent reports have demonstrated activities that dramatically surpass the proposed performance targets (0.44 A mg_{Pt}^{-1} DOE target).[4,6−8] However, these excellent performances are yet to be translated to the real application. One of the major drawbacks of Pt-alloy (Pt−M) electrocatalysts is the insufficient stability of M at the ORR working potentials in acidic PEMFC environment,[9] which results in leaching/dealloying of M.[10−12] Although some corrosion is initially even desired to form a Pt-rich overlayer over the PtM_x core and enhance the ligand and/or strain effect, any further corrosion—especially in the membrane electrode assembly (MEA) environment—leads to significant drop of ORR specific activity.[13] In a previous study by General Motors,[14]

Received: December 8, 2018
Accepted: April 16, 2019
Published: April 16, 2019

the MEA performance of a Pt−Cu/C and a Pt−Co/C electrocatalyst has been compared. Both electrocatalysts were acid leached prior to MEA fabrication to achieve sufficient removal of the sacrificial less-noble-metal. Initially, the Pt−Cu/C electrocatalyst outperformed the Pt−Co/C analogue. However, further stability testing caused dealloying of additional amounts of M (M = Cu or Co). In the case of Pt−Co/C electrocatalyst, the MEA-*in-operando*-dissolved metal ions resulted only in a drop of specific activity (most likely because of the weakening of ligand or strain effect). By contrast, the effect was much more devastating in the case of Pt−Cu/C electrocatalyst: Cu^{2+} ions were shown to interact with both the electrodes, as well as the membrane—worsening significantly the PEMFC performance over time.[14]

While it is well-known that subsurface atomic structure defines the Pt-alloy ORR activity,[13,15,16] the importance of surface impurities (M) is often overlooked.[17,18] M can interact with the Pt surface either via noncovalent interactions[19,20] or via electrodeposition, also referred to as the overpotential deposition (OPD) or the phenomenon of underpotential deposition (UPD).[9] In the case of UPD, the deposited species usually cover the substrate metal surface in the form of up to one monolayer. Importantly, it occurs at potentials more positive compared to the OPD of less-noble-metals.[21] For Cu on Pt these potentials are 0.34 V_{RHE} (OPD) and 0.45/0.6−0.7 V_{RHE} (UPD),[22,23] whereas for Co on Pt the respective values are −0.45 V_{RHE} (OPD) and 0.5 V_{RHE}(UPD).[9] In one of the rare studies,[21] it was shown that Cu at concentrations as low as 10 μM (subsequently acting as OPD and UPD species) can dramatically worsen electrocatalytic performance of Pt nanoparticles by drastically inhibiting the hydrogen oxidation reaction (HOR). Additionally, as part of the same study, Cu adatoms were shown to impact the mechanism of ORR at the cathode side by changing the four-electron pathway of ORR to two-electron mechanism (peroxide production).[18,21] Further insights in Pt−Cu interaction were obtained by X-ray absorption (XAS) revealing presence of Cu at the surface at potentials even as high as 0.84 V_{RHE}—for example, potentials relevant for operating conditions of PEMFC.[21] Furthermore, a study by Durst et al. provides insight into vastly different behavior of M in the presence of either Pt surface|polymer(Nafion)|liquid interface (such as typically found in TF-RDE) or Pt surface|polymer(Nafion)|gas interface (such as typically found in PEMFC).[19] Not taking into account this important fact may lead to erroneous conclusions as regards the effect of interaction between M and Pt in the surface layer, which is expected to be highly significant.[14,19,21,24]

In the present work, the interaction between M and Pt is investigated through dissolution dynamics of M which could help explain why Pt−Cu and Pt−Co ORR electrocatalysts behave differently. This is targeted by using highly sensitive online measurements of electrochemically dissolved Pt, Cu, and Co in a configuration of electrochemical flow cell (EFC) connected to an inductively coupled plasma mass spectrometer (ICP-MS).[12,25−28] For this purpose, the following electrocatalysts are investigated: (i) in-house designed, highly active Pt−Cu nanoparticles dispersed on high surface area carbon (hereinafter referred to as Pt−Cu/C electrocatalyst) and (ii) the state-of-the-art commercial benchmark alloy catalyst consisting of Pt−Co nanoparticles on high surface area carbon (TEC36E52, Tanaka, Japan, hereinafter referred to as Pt−Co/C electrocatalyst). Dissolution dynamics obtained by the EFC-ICP-MS methodology are complementary compared to the TF-RDE ORR performances and provide new insight into surface dynamics of M (Cu or Co).

EXPERIMENTAL SECTION

Synthesis. *Pt−Cu/C.* Intermetallic ordered $PtCu_3$ nanoparticles that are tightly embedded (anchored) into a modified carbon support were prepared via patented, but upgraded modified sol−gel synthesis using a gelatin precursor.[13,29−31] Briefly, the synthesis consists of two vital steps, the first being annealing of a Cu salt precursor together with gelatin and carbon black to obtain Cu particles in a porous carbon matrix. In the second part, the Cu from the composite is partly galvanically displaced by a Pt precursor (K_2PtCl_4) and annealed for the second time. The "as prepared" Pt−Cu/C electrocatalyst was prepared in a 2 g batch.

Pt−Co/C (TEC36E52). The electrocatalyst has not been modified prior to any electrochemical measurements and was used "as received". The electrocatalyst already shows evidence of acid leaching (visible porosity on larger particles) in the "as received" state (see Figure S5).

XRD Analysis. The powder X-ray diffraction (XRD) measurements of all samples were carried out on a Siemens D5000 diffractometer with Cu Kα1 radiation (λ = 1.5406 Å) in the 2θ range from 10° to 60° with the 0.04° step per 1 s. Samples were prepared on zero-background Si holder.

TEM Analysis. Transmission electron microscopy (TEM) was carried out in a probe Cs-corrected scanning transmission electron microscope Jeol ARM 200 CF equipped with an SDD Jeol Centuria Energy-dispersive X-ray (EDX) spectrometer. The operational voltage was set to 200 kV. High-angle annular dark field (HAADF) images were taken with 68 and 180 mrad for inner and outer semiangles. Convergence angle was set to 25 mrads.

Electrochemical Evaluation via Thin Film Rotating Disc Electrode (TF-RDE). *Preparation of Thin Films and the Setup.* Electrochemical measurements were conducted in a two-compartment electrochemical cell in a 0.1 M $HClO_4$ (Merck, Suprapur, 70%, diluted by Milli-Q, 18.2 MΩ cm) electrolyte with a conventional three-electrode system controlled by a potentiostat (CompactStat, Ivium technologies). Ag|AgCl was used as a reference and a Pt wire as a counter electrode. The working electrode was a glassy carbon disc embedded in Teflon (Pine Instruments) with a geometric surface area of 0.196 cm^2. The Ag|AgCl reference was separated from both the working and the counter electrode via a salt bridge to avoid Cl^- ions contamination. Prior to each experiment, the two-compartment electrochemical cell was boiled in Milli-Q water for 1 h, and the electrode was polished to mirror finish with Al_2O_3 paste (particle size 0.05 μm, Buehler) on a polishing cloth (Buehler). After polishing, the electrodes were rinsed and ultrasonicated (Ultrasound bath Iskra Sonis 4) in Milli-Q water for 5 min. Twenty microliters of 1 mg mL^{-1} water-based well-dispersed electrocatalysts ink was pipetted on the glassy carbon electrode completely covering it and dried under ambient conditions. After the drop had dried, 5 μL of Nafion solution (ElectroChem, 5% aqueous solution) diluted in isopropanol (1:50) was added. Such preparation resulted in the electrocatalyst loading of 20 μg for both electrocatalysts and a loading of approximately 6.2 μg_{Pt} cm^{-2}_{geo} in the case of Pt−Cu/C electrocatalyst and 47 μg_{Pt} cm^{-2}_{geo} in the case of Pt−Co/C electrocatalyst.

Electrochemical Potential Hold Activation. After it was dried, the electrode was mounted on a rotator (Pine Instruments). The electrode was placed in Ar saturated electrolyte under potential control at 0.05 V_{RHE}. Both electrocatalysts were first subjected to a potential hold activation (0.6 V_{RHE}) for 30 min under the rotation rate of 600 rpm (hereinafter referred to as PHA). After PHA activation, the electrolyte was exchanged with a fresh one. ORR polarization curves were measured in an oxygen saturated electrolyte with a rotation rated at 1600 rpm in the potential window 0.05−1.0 V_{RHE} with a scan rate of 20 mV s^{-1}. At the end of ORR polarization curve measurement, the electrolyte was purged with CO under potentiostatic mode (0.05 V_{RHE}) to ensure successful CO adsorption. Afterward the electrolyte was saturated with Ar. CO electrooxidation

DOI: 10.1021/acsaem.8b02142
ACS Appl. Energy Mater. 2019, 2, 3131−3141

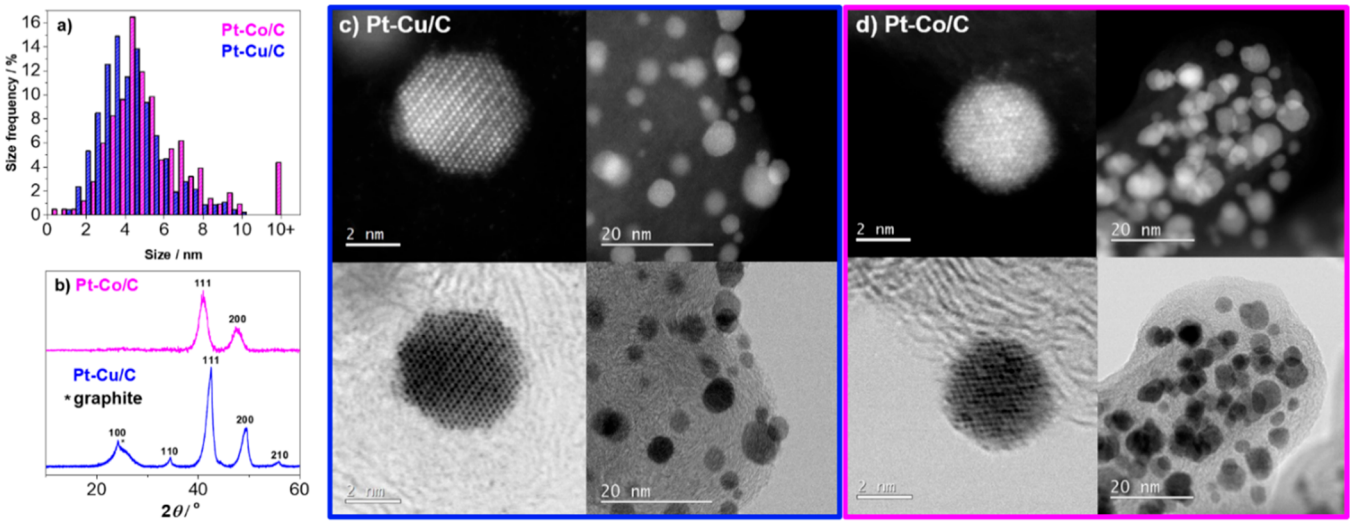

Figure 1. Structural and morphological characterization of the electrocatalysts used in this study. (a) Size distributions, (b) XRD spectra, and (c, d) representative STEM/HAADF images of both electrocatalysts (Pt−Cu/C in "as prepared" state and Pt−Co/C in "as received" state). For additional TEM analysis see Figures S1−S5.

was performed using the same potential window and scan rate as in ORR but without rotation and in an Ar saturated electrolyte. Electrochemical surface area (ESA) was determined by integrating the charge in CO electrooxidation experiments as described in ref 32. After subtraction of background current because of capacitive currents, kinetic parameters were calculated at 0.9 V_{RHE}. Ohmic resistance of the electrolyte was determined and compensated for as reported in ref 33.

Electrochemical Potential Cycling Activation. Both electrocatalysts were electrochemically activated for 200 cycles between 0.05 and 1.2 V_{RHE} with a scan rate of 300 mV s^{-1} under a rotation rate of 600 rpm (hereinafter, referred to as PCA). After PCA, the electrolyte was once again exchanged for a fresh one. All potentials are given against the reversible hydrogen electrode (RHE), which was measured before the start of the experiment and at the end. ORR polarization curves (including ohmic resistance and compensation), and CO stripping measurements were repeated using the same process as described above.

EFC-ICP-MS. *Electrochemical Flow Cell Setup.* The working and counter electrodes in the electrochemical flow cell (EFC) were glassy carbon discs (3 mm diameter) embedded into PEEK material (BASi). The discs were aligned in series; the counter electrode was placed first and the working electrode second in the direction of the electrolyte flow. The sample was deposited on the electrode by drop casting 5 μL drop of the ultrasonically homogenized catalyst ink (1 mg mL^{-1}). Such preparation resulted in the electrocatalyst loading of 5 μg for both electrocatalysts and a loading of approximately 4.3 μg_{Pt} cm^{-2}_{geo} in the case of Pt−Cu/C electrocatalyst and 32.8 μg_{Pt} cm^{-2}_{geo} in the case of Pt−Co/C electrocatalyst. After the drop had dried, 5 μL of Nafion solution (ElectroChem, 5% aqueous solution) diluted in isopropanol (1:50) was added. The Ag|AgCl reference electrode potential against RHE was determined before the start of the experiment. The housing of the cell was made from PEEK material and the design was modeled after a commercial cross-flow cell (BASi, MF-1092, cross-flow cell). The volume of the cell was established with a homemade silicon gasket with 1.0 mm thickness and 1.5 cm^2 ellipsoidal cut. For better visualization of the setup see Scheme S1. The carrier solution (0.1 M $HClO_4$) was pumped through the cell at a constant flow of 400 μL min^{-1}. Two glass syringes, two syringe pumps (WPI sp100i and Harward apparatus 11 PLUS) and a diagonal 4-way flow valve (Idex, V-100D) were used to enable a continuous flow of the solution.

ICP-MS. The EFC was coupled with an ICP-MS detector, namely, Agilent 7500ce ICP-MS instrument (Agilent Technologies, Palo Alto, CA), equipped with a MicroMist glass concentric nebulizer and a Peltier cooled Scott-type double-pass quartz spray chamber. A forward radio frequency power of 1500 W was used with Ar gas flows: carrier 0.85 L min^{-1}; makeup 0.28 L min^{-1}; plasma 1 L min^{-1}; and cooling 15 L min^{-1}. The signals were recorded for Co_{59}, Cu_{63}, and Pt_{195} with 0.3 s integration per data point. To convert the ICP-MS signals to concentration (ppb), standard solution of Cu, Co, and Pt in 0.1 M $HClO_4$ were recorded with the following concentrations: 0.5, 1, 2, 5, 10, 20, 50, 100, and 200 ppb.

Electrochemical Protocol. Electrochemical experiments were performed with a BioLogic SP-300 potentiostat with a typical three-electrode setup. No ohmic drop compensation was used. Initially, Milli-Q water was pumped through the cell and potential control (0.05 V_{RHE}) was established 3 min prior to switching the carrying solution to 0.1 M $HClO_4$. After 5 min of acid flow, the electrochemical activation protocol was started; either potential cycling (200 cycles between 0.05 and 1.2 V_{RHE} with a scan rate of 300 mV s^{-1}) or potential hold (0.6 V_{RHE}, 30 min) activation. Subsequently, 10 min of OCP was allowed before performing slow potential cycles from 0.05 V_{RHE} to increasing upper-potential limit (UPL). Three cycles were repeated in each potential window. Either 20 mV s^{-1} or 5 mV s^{-1} scan rate was used. The protocol with the 20 mV s^{-1} scan rate had the UPLs 1.0, 1.1, 1.2, 1.3, and 1.4 V_{RHE}, while the UPLs of 5 mV s^{-1} scan rate were 1.0, 1.2, and 1.4 V_{RHE}. After each experiment a sequence of potential pulses was performed in order to synchronize the electrochemical experiment with the ICP-MS signal. For details see Tables S1−S3, for the differences in the chemical compositions between Pt−Cu/C and Pt−Co/C electrocatalysts after PCA see Figure S1 and for the reproducibility of the EFC-ICP-MS measurements, see Figure S6.

RESULTS AND DISCUSSION

The mail goal of the present study is to elucidate the mechanistic differences in dealloying of M and its surface interactions with Pt. For this purpose, two well-defined Pt-alloy-based carbon-supported electrocatalysts are compared—an in-house designed Pt−Cu/C electrocatalyst and a commercial Pt−Co/C benchmark electrocatalyst.

It is important to note that while ideal, such a comparison can hardly be carried out on samples with identical composition and/or morphologically features—one of many reasons being largely different alloy thermodynamics (phase diagrams), which, in turn, for example, require different thermal treatment of both alloys to obtain electrocatalysts with reasonably good electrochemistry. The present in-house

DOI: 10.1021/acsaem.8b02142
ACS Appl. Energy Mater. 2019, 2, 3131−3141

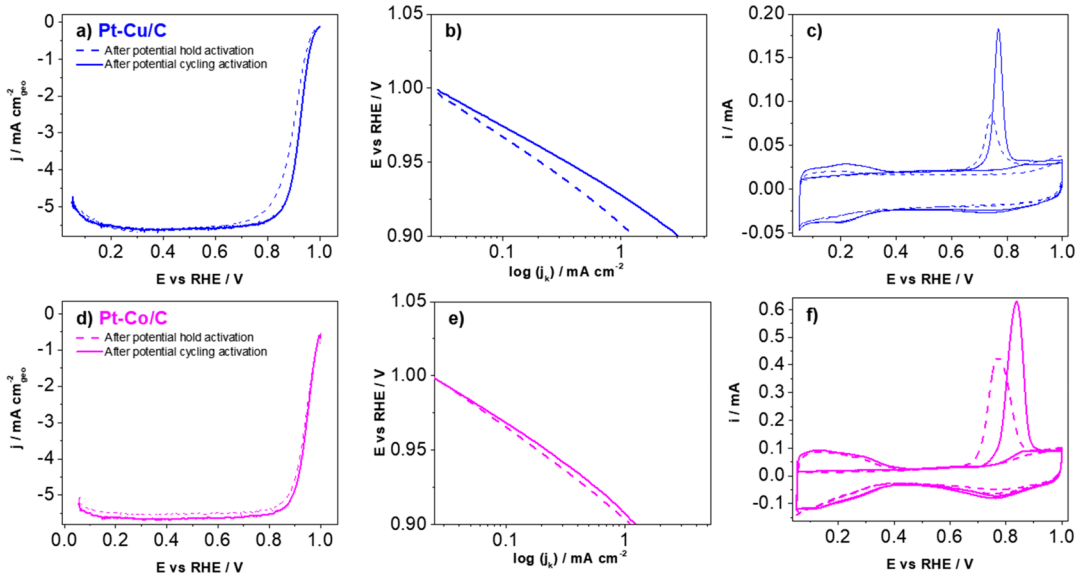

Figure 2. (a, d) ORR polarization curves (0.1 M $HClO_4$, 20 mV s^{-1}, 1600 rpm, ohmic resistance compensated), (b, e) Tafel plots, and (c, f) CO electrooxidation experiments (with the follow-up cycle; 0.1 M $HClO_4$, 20 mV s^{-1}, no rotation) of our Pt−Cu/C and Pt−Co/C electrocatalysts after PHA (dashed lines) and after PCA (full lines). The CVs for both electrocatalysts obtained during PCA are presented in Figure S7, while Tafel slopes after PHA and after PCA can be found in Table S4. Statistically relevant measurements for both Pt−Cu/C and Pt−Co/C (TEC36E52) as well as Pt/C (TEC10E50E-HT) after PCA can be found in Figure S9.

synthesis method was thus not used for preparation of Pt−Co/C electrocatalyst and a well-defined and active commercial reference was used for comparison instead. To account for the complex nature of structure−stability relationship, such as crystal structure ordering[34−36] or particle size effect,[37] we carry out rather detailed structural and morphological analysis and comment on the observed similarities and differences.

Both analogues have similar particle size distributions (Figure 1a); however, the Pt−Cu/C electrocatalyst still has a higher fraction of sub 5 nm particles, as well as a smaller fraction of particles larger than 10 nm which results in a big difference in electrochemically active surface area (ESA) (see Table S5). Furthermore, there are other differences between the electrocatalysts. For example, the Pt loading of Pt−Cu/C electrocatalyst is much lower−only 6.1 wt % in the "as prepared" state, while the commercial Pt−Co/C electrocatalyst has a Pt loading of 46.3 wt % in the "as received" state. XRD analysis of Pt−Cu/C (Figure 1b) reveals a peak at around 25° 2θ that corresponds to the graphitic nature of our modified carbon support. This peak is absent in the case of commercial Pt−Co/C. However, TEM analysis (Figure 1c and d) shows that both carbon supports have an "onion-like" structure pointing toward the graphitic nature of both carbon supports.[38−40] In the case of Pt−Cu/C, both TEM and XRD analysis (Figures 1b and c) consistently show the presence of an ordered $Pm\bar{3}m$ structure, which is not present in Pt−Co/C. While the overall composition of the latter is roughly Pt_3M, the transition metal (Cu) largely predominates in the present Pt−Cu/C electrocatalyst with a general formula PtM_3. Additionally, while our Pt−Cu/C electrocatalyst was used in the "as prepared" state (no preleaching was carried out), the Pt−Co/C electrocatalyst was used "as received". In other words, the Pt−Co/C electrocatalyst had been subjected to a specific ex situ activation by the producer (unfortunately the details are not available, see also Figure S5). Interestingly, despite the different history, both electrocatalysts lose significant amounts of their less-noble-metal component during the present activation protocols (see Figure S1), as well as form a very similar Pt-rich overlayer (see Figure S2). The differences summarized above will be appropriately accounted for when evaluating and comparing the behavior of both electrocatalysts.

TF-RDE Characterization. To inspect the electrochemical performance of the present electrocatalysts, a TF-RDE analysis of both samples was initially performed by employing two different activation procedures, namely the potential hold activation (PHA)[12] and the potential cycling activation (PCA)[35] protocols. These were chosen to exemplify the effect of M. After the PHA, the initial ORR specific activity of Pt−Cu/C at 0.9 V_{RHE} was relatively low (1.30 mA cm^{-2}), while additional PCA led to a more than 200% improvement (2.62 mA cm^{-2}) as shown in Figure 2a and b (see also Figure S7a and Table S5a). However, only upon PCA, an excellent ORR activity of the Pt−Cu/C electrocatalyst was achieved, especially when compared to the Pt−Co/C and Pt/C commercial samples having specific activities of 1.14 and 0.44 mA cm^{-2} after PCA, respectively (see Figure S7b and Table S5b, as well as Figure S8 and Table S6). Additionally, an in-depth discussion related to the comparison of the ORR mass activities between Pt−Cu/C, Pt−Co/C and Pt/C electrocatalysts measured after PCA is available in the text related to Figure S9. This could indicate that PCA, in contrast to PHA, ensured a more efficient removal of unstable subsurface Cu. We presume this resulted in a lower degree of Cu dealloying in each cycle after PCA and subsequently a lower degree of coverage with Cu_{UPD} that can block the active Pt surface and inhibit ORR. We observed almost no difference in the low overpotential region which indicates that in this region both PHA and PCA treatments resulted in a similar ORR activity. This is in line with the fact that in this potential region the coverage with Cu (θ_{Cu}) is negligible (the surface is almost completely covered with OH_{ad} species; Figure 2b and see also Supporting Information, Table S4 for Tafel slope values). To get a further understanding of the effects of Cu ions on ORR, we performed an additional experiment on Pt/C

DOI: 10.1021/acsaem.8b02142
ACS Appl. Energy Mater. 2019, 2, 3131−3141

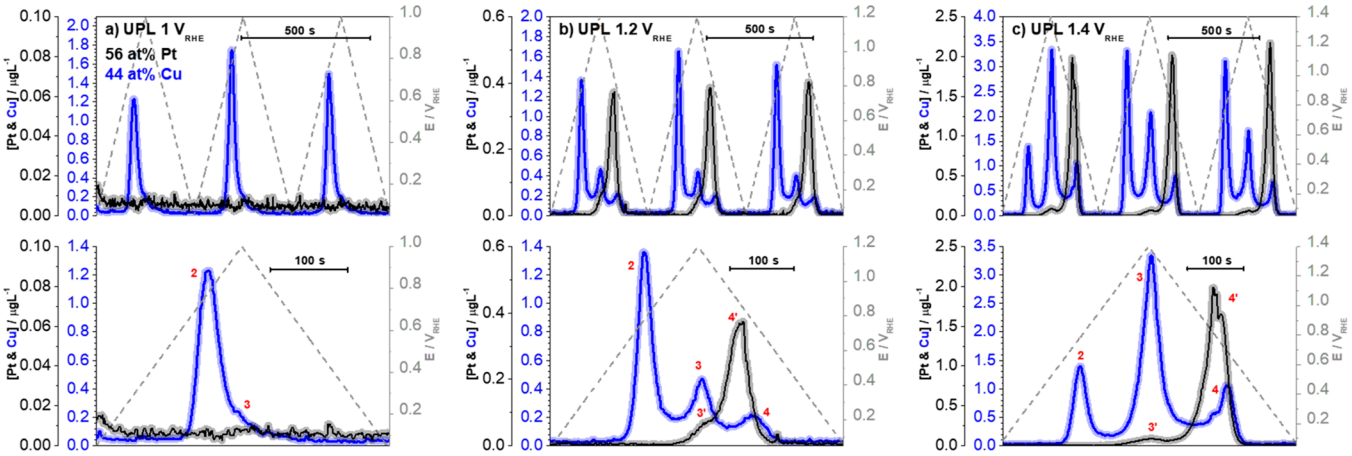

Figure 3. (a–c) EFC-ICP-MS measurements of metal dissolution (Pt and Cu) for our in-house designed Pt–Cu/C electrocatalyst after PCA during slow cycles (0.1 M $HClO_4$, 5 mV s^{-1}, 0.05–1.*X* V_{RHE}, *X* = 0, 2, and 4). Three consecutive cycles (upper graphs) and details within a single cycle (lower graphs) for the upper potential limits (1.0, 1.2, and 1.4 V_{RHE}) are displayed. Peak 2 corresponds to Cu_{UPD}, while peaks 3 and 4 correspond to anodic and cathodic corrosion of Pt and Cu, respectively. Each metal has its own *Y* axis to better compare the dissolution profiles despite the detected concentration differences.

electrocatalyst (TEC10E50E-HT, see Figure S10) whereby ORR polarization curves in absence and in the presence of different concentrations of Cu ions were measured. The ORR polarization curve exhibited a similar trend as found in the case of Figure 2a, while the effect on the overpotential was again negligible. A further insight in the underlying mechanism can be obtained by comparing CO electrooxidation curves, as well as the follow-up cycles. Namely, a clear and significant difference is visible between CO electrooxidation peak obtained after PHA and the one obtained after PCA (Figure 2c). In general, for both electrocatalysts, the onset of CO electrooxidation is shifted toward more negative potentials after PHA (in other words, it seems that the shift of the onset is independent of the type of alloying element itself). One explanation for the shift in the CO electrooxidation onset potential is a difference in surface roughness.[41] However, we once again performed an additional experiment on the Pt/C electrocatalyst (TEC10E50E-HT, see Figure S11) in which we compared CO electrooxidation curves, together with the follow-up cycles, in absence and in the presence of different concentrations of Cu ions. Both the results on Pt-alloy electrocatalysts, as well as the supporting experiment on the Pt/C electrocatalyst (TEC10E50E-HT) indicate that the shift in the onset is most likely a consequence of the presence of the less-noble metal. Durst et al. have shown that metal cations result in a more facile (hydr)oxide formation at the Pt surface induced by less-noble-metal cations (both Cu^{2+} and Co^{2+}) in the double layer.[19] Hydrated cations are located between the inner and outer Helmholtz plane where they partially lose their hydration shell and come closer to the Pt surface, yielding increased OH_{ad} coverage that can cause the shift in the onset of CO electrooxidation.[20] In addition, the CO electrooxidation peak and both the hydrogen underpotential deposition (HUPD) region and the Pt-oxide formation and reduction region of the follow-up cycle are also much less pronounced after PHA in contrast to PCA (Figure 2c). This also indicates a higher degree of surface blockage after PHA with Cu species (Cu_{UPD} or even Cu_{OPD}).[42]

In contrast to the Pt–Cu/C electrocatalyst, the Pt–Co/C counterpart exhibits almost insignificant difference (within the margin of error) in specific activity at 0.9 V_{RHE}—from 1.10 mA cm^{-2} measured after PHA to 1.14 mA cm^{-2} measured after PCA (Figure 2d, e and Table S5b). Surprisingly such a large amount (i.e., as much as 40 at%) of dissolved total Co from Pt–Co/C electrocatalyst (see Figures S1 and S12) did not result in a change of ORR activity (which could either be better due to a lower degree of dealloying of Co per cycle or worse—due to expected loss of ligand or strain effect). This indicates that Pt–Co/C is much less prone to the UPD interaction of the less-noble-metal at the Pt surface|polymer-(Nafion)|liquid interface, and thus to a smaller degree of surface blockage than the Pt–Cu/C counterpart. Similarly as in the case of Cu, the rather intense dissolution of Co should worsen the PEMFC performance due to the higher OH_{ad} coverage of Pt induced by Co^{2+} ions at the Pt surface|polymer(Nafion)|gas interface where Co^{2+} ions reach the inner Helmholtz plane.[19] In the case of PHA a similar shift in the onset of CO electrooxidation toward more negative potentials (Figure 2f) can also be observed for Pt–Co/C electrocatalyst (again due to a Co^{2+} ions).[19] Again, this implies a higher degree of noncovalent interactions. The value of ESA_{CO} measured after both activation protocols also remained within the margin of error (see Table S5b). This—together with the fact that both HUPD and Pt-oxide features are much more pronounced than in Pt–Cu/C already after PHA—again proves that the Pt–Co/C electrocatalyst is much less prone to surface blockage (UPD interaction) by its less-noble-metal component than the Pt–Cu/C electrocatalyst.

EFC-ICP-MS Characterization of Pt–Cu/C Electrocatalyst. To better understand the differences observed in TF-RDE measurements, further investigation was performed using the electrochemical flow cell connected to an ICP-MS device (EFC-ICP-MS). As in the case of TF-RDE characterization, the electrocatalysts were first subjected to an electrochemical activation protocol (either PHA or PCA). Slow potentiodynamic treatment followed the activation protocol to obtain clearly resolved dissolution profiles. Figure 3 shows examples of dissolution profiles of Pt and Cu after PCA (see also Figure S12a) during slow potentiodynamic cycles. During the anodic scan, the Cu dissolution profile (Figure 3a, upper graph) reveals a single, clearly resolved peak. However, upon careful inspection of a single slow scan (Figure

DOI: 10.1021/acsaem.8b02142
ACS Appl. Energy Mater. 2019, 2, 3131–3141

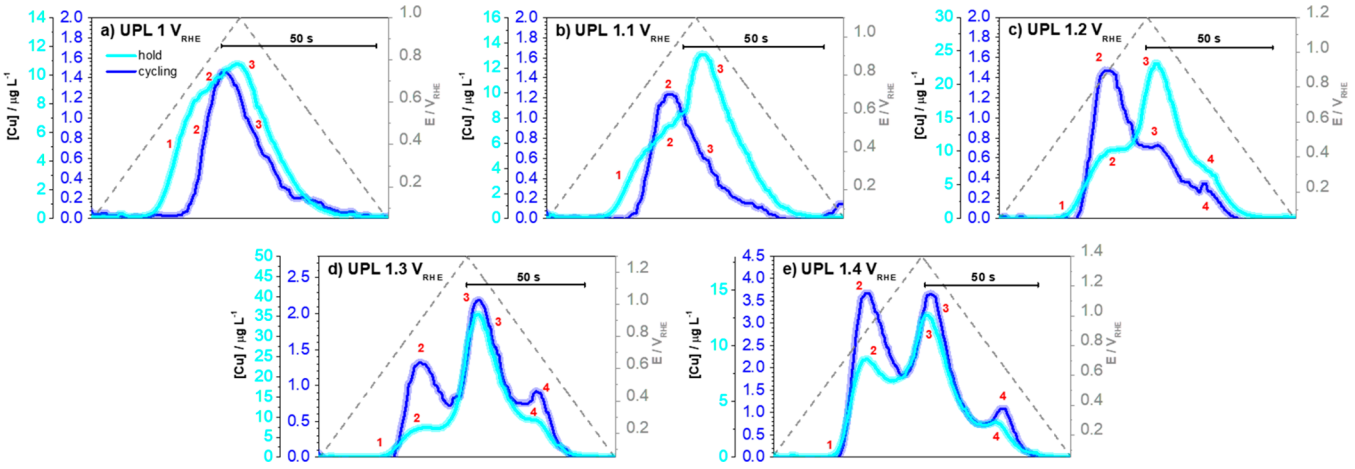

Figure 4. (a–e) EFC-ICP-MS measurements of Cu dissolution for our in-house designed Pt–Cu/C electrocatalyst after either PHA or after PCA during slow cycles (0.1 M $HClO_4$, 20 mV s^{-1}, 0.05–1.*X* V_{RHE}, *X* = 0, 1, 2, 3, and 4). Peak 1 corresponds to Cu_{OPD}, peak 2 corresponds to Cu_{UPD}, while peaks 3 and 4 correspond to anodic and cathodic corrosion of Cu. Each activation protocol has its own *Y* axis to better compare the dissolution profiles despite the detected concentration differences.

3a, bottom graph), another Cu dissolution feature (shoulder peak 3) positioned at the upper potential limit (UPL) is observed. Peak 2 with the onset of approximately 0.6 V_{RHE}[9] presents a stripping process of Cu_{UPD} from Pt surface,[21,43] while peak 3 is ascribed to the well-known anodic Cu dissolution (dealloying, Cu_{anodic}) from Pt–Cu subsurface alloy.[12] Intriguingly, even after PCA, the Cu signal detected at peak 2 is much higher than the shoulder peak 3. The absence of Cu_{OPD} (peak 1) as well as a low degree of Cu_{anodic} (peak 3) can be considered as good indicators of successful activation protocol in the case of Pt–Cu alloy system (either ex situ chemical or in situ electrochemical). Figures 3b and c show dissolution profiles of Pt and Cu upon increasing the UPL to 1.2 and 1.4 $V_{RHE,}$ respectively. Apart from the already mentioned peaks corresponding to Cu_{UPD} and Cu_{anodic}, we notice appearance of an additional Cu dissolution peak 4 ($Cu_{cathodic}$), as well as peaks 3′ and 4′ corresponding to anodic and cathodic dissolution of Pt (Pt_{anodic} and $Pt_{cathodic}$). This is a consequence of the reduction of Pt-oxide which is accompanied by restructuring of Pt surface and subsurface as well as intensive Pt cathodic dissolution—the so-called oxide place exchange.[44] Upon careful inspection of a single slow scan (Figure 3b and c, bottom), we notice that Pt_{anodic} and Cu_{anodic} take place simultaneously (in other words, the maxima of peak 3-Cu_{anodic} and peak 3′-Pt_{anodic} are aligned). We could speculate that the oxide place exchange[44] simultaneously triggers Cu_{anodic}. On the other hand, the reduction of the Pt-oxide accompanied by $Pt_{cathodic}$ seems to trigger subsequent removal of the less-noble component (in other words, the onset of peak 4-$Cu_{cathodic}$ occurs after the onset of peak 4′-$Pt_{cathodic}$).[26,44,45] Furthermore, a careful inspection of three consecutive cycles to the UPL of 1.4 V_{RHE} (Figure 3c, upper graph) reveals another phenomenon that might explain the quite significant levels of Cu_{UPD} (Peak 2). While in the first cycle up to UPL of 1.4 V_{RHE} the signals corresponding to peaks 2 (Cu_{UPD}) and 4 ($Cu_{cathodic}$) (Figure 3c) show similar levels of Cu dissolution intensity, an increase in peak 2 (Cu_{UPD}) and decrease in peaks 3 (Cu_{anodic}) and 4 ($Cu_{cathodic}$) is clearly detected in the following two cycles. Both Pt_{anodic} and $Pt_{cathodic}$ are damaging the protective Pt surface layer (at higher UPLs the damage by $Pt_{cathodic}$ clearly prevails), which causes dealloying of fresh subsurface Cu as Cu_{anodic} and $Cu_{cathodic}$. Some of this Cu is redeposited back to the Pt surface as Cu_{UPD}. This Cu is then stripped and detected in the next cycle as peak 2 (Cu_{UPD}). This might explain the increasing dissolution trend corresponding to peak 2 within the three cycles (Figure 3b, c). In short, one may speculate that the actual dissolution mechanism is masked by the favorable Pt–Cu interaction (Cu_{UPD}). Furthermore, the rather strong presence of Cu_{UPD} provides an intriguing question: What is the intrinsic activity of dealloyed $PtCu_3$ nanoparticulate system? In a model study by Bandarenka et al.[46] it was demonstrated that the Pt–Cu system should exhibit a superior activity enhancement in comparison to other Pt-alloy systems. Experimentally, however, the Pt–Ni system seems to be have the best performance.[4,6,7] On the other hand, we observe that the activity of the present in-house Pt–Cu/C electrocatalyst is highly dependent on the activation protocol itself (Figure 2a,b), which is not the case for the Pt–Co/C electrocatalyst (Figure 2d,e). In addition, the present Pt–Cu/C alloy shows a distinct superiority in terms of measured specific activity after PCA in comparison to many reports on other variants of Pt–Cu nanoparticulate systems found in the literature.[14,47−50]

Several effects associated with the use of Cu-based Pt alloys in electrocatalytic applications have been identified in the literature, such as the negative impact on long-term MEA performance[14] or the effects of Cu_{OPD} and Cu_{UPD} on the performance of Pt/C in TF-RDE setup.[21] This study importantly complements the previous findings by providing detailed Cu dissolution profiles obtained during slow potentiodynamic cycles, as well as a correlation with their ORR performance after two different activation protocols—PHA and PCA. Upon comparison of both protocols, Figure 4 reveals that the peaks of Cu dissolution profiles measured after each activation protocol do not overlap. Furthermore, for every UPL, there is about an order of magnitude higher signal for Cu dissolution in the case of PHA in comparison to PCA. Additionally, in the case of PHA, we notice the presence of Peak 1 with an onset potential of 0.37 $V_{RHE,}$ which corresponds to the dissolution of Cu_{OPD}—presence of Cu multilayers—and is absent in the case of PCA.[9] Figures 3 and 4 thus clearly support the main finding of Figure 2a and b, namely, that both protocols have a decisively different impact on ORR activity of Pt–Cu/C electrocatalyst which is a consequence of a profoundly different degree of dealloying of Cu. In other

DOI: 10.1021/acsaem.8b02142
ACS Appl. Energy Mater. 2019, 2, 3131−3141

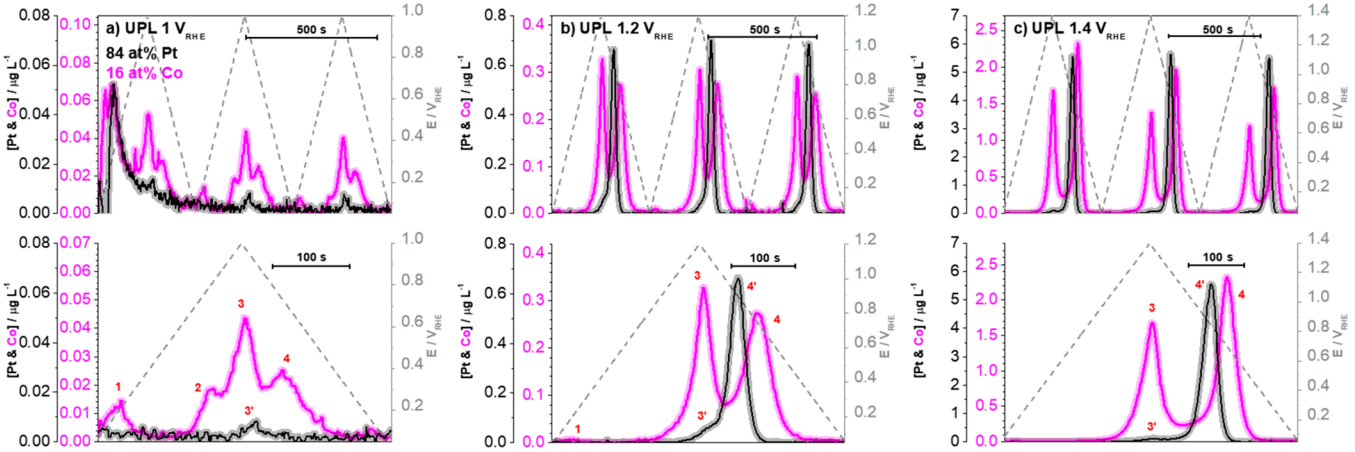

Figure 5. (a–c) EFC-ICP-MS measurements of metal dissolution (Pt and Co) for the commercial Pt–Co/C electrocatalyst after PCA during slow cycles (0.1 M $HClO_4$, 5 mV s^{-1}, 0.05–1.*X* V_{RHE}, *X* = 0, 2, and 4). Each showcase three consecutive cycles, as well as a more careful inspection of a single cycle for each of the upper potential limits (1.0, 1.2, and 1.4 V_{RHE}). Peak 1 corresponds to Co_{OPD}, peak 2 to Co_{UPD}, while peaks 3 and 4 correspond to anodic and cathodic corrosion of Pt and Co, respectively. Each metal has its own *Y* axis to better compare the profiles despite the detected concentration differences.

words, more dealloying of Cu from the Pt–Cu nanoparticles crystal structure results in a higher degree of Cu_{UPD} interaction that blocks the active surface.[21] This further helps explain the observed difference in the Tafel slopes (Figure 2b, see also Table S4), where the higher Cu_{UPD} coverage changes the slope. In summary, (i) in contrast to potential-cycling-activated Pt–Cu/C electrocatalyst, the potential-hold-activated Pt–Cu/C electrocatalyst is dealloying an order of magnitude higher amounts of Cu with every slow cycle, regardless of the UPL (Figure 4). (ii) Dealloyed Cu can interact with the Pt surface via noncovalent interactions or in the form of surface-blocking Cu_{UPD}—to the point of also forming multilayers of Cu (Cu_{OPD}). (iii) In the case of PHA, the noncovalent interactions of Cu ions are most likely responsible for the more facile CO electrooxidation (Figure 2c); by contrast, surface blockage (UPD interaction) is responsible for the less-pronounced CO electrooxidation peak, as well as less pronounced HUPD and Pt-oxide features in the follow-up cycle. Additionally, in the case of PHA, Pt surface is being blocked by a much higher amount of Cu than in the case of PCA, resulting in a lower ORR specific activity at 0.9 V_{RHE}. (iv) The goal of an activation protocol in Cu-based Pt-alloy electrocatalysts therefore should be to deplete the near surface area of unstable Cu. Effectively, this can be done by creating an appropriately thick (e.g., a few monolayers) Pt-rich overlayer (see Figure S2). An optimally thick and for the most part Cu-depleted Pt-rich overlayer should prevent further excessive dealloying of Cu from subsurface regions, while not compromising the activity improvement from the ligand or strain effect. A good indication for the success of an activation protocol (be it ex situ chemical or in situ electrochemical) can be obtained by measuring EFC-ICP-MS less-noble-metal dissolution profiles. (v) Peak 2 (Cu_{UPD}) is the dominant dissolution peak after PCA until UPL 1.4 V_{RHE} (Figure 3). This means that a significant part of anodically or cathodically dissolved Cu ends up interacting with the surface in the form of Cu_{UPD}. (vi) The unusually wide range of reported activities in the case of Pt–Cu/C systems[14,47−50] could be a direct consequence of poor control of the Pt–Cu surface interaction using inadequate activation protocols. (vii) As regards to possible application of the present findings on a commercial level, one might consider to drastically reduce the degree of operando Cu dealloying/leaching (for example via Au doping[12,51−53]) or effectively avoid any potential jumps above 1 V_{RHE}[54,55] (e.g., due to start–stop conditions[56,57]), where Cu_{anodic} or $Cu_{cathodic}$ can become significant. This could prevent or at least partly mitigate the scenario presented in the work by Yu et al, where Cu was found to not only significantly dealloy from Pt–Cu nanoparticles (despite ex situ chemical activation prior to MEA implementation) but also plate the anode by migrating through the membrane, which resulted in a drastic inhibition of HOR.

EFC-ICP-MS Characterization of Pt–Co/C Electrocatalyst. Figure 5 showcases obtained dissolution profiles of Pt and Co after PCA (see Figure S12b) during slow potentiodynamic cycles. According to the literature, the onset for Co_{OPD} dissolution occurs at −0.45 V_{RHE}.[9] Since in our case the potentials are always above the onset of Co_{OPD}, we do not detect this type of dissolution. Nevertheless, a small peak 1 is in-fact present (Figure 5a). We speculate that this peak could correspond to the dissolution of Co_{OPD} or alternatively Co_{UPD}. A small peak 2 with the onset at approximately 0.5 V_{RHE} was also detected and could be referred to as Co_{UPD}, as already shown in the literature.[58,59] We note that the reports of Co_{UPD} on Pt are very scarce. A maximum of 0.6 monolayer coverage is possible in 0.1 M H_2SO_4.[43] Furthermore, as visible in Figure 5a, peak 2 rapidly disappears and becomes almost negligible in the second and third cycle. At more positive potentials with the peak maximum at the UPL, another Co dissolution peak is detected (Figure 5a, peak 3). By analogy to Cu, it is ascribed to anodic Co dissolution (dealloying) from the Pt–Co alloy subsurface (Co_{anodic}). Rather surprisingly, already at the UPL of only 1.0 V_{RHE} (Figure 5a), we have also detected peak 4 ($Co_{cathodic}$). As discussed in the case of our Pt–Cu/C electrocatalyst, the cathodic corrosion of the less-noble component is a consequence of $Pt_{cathodic}$. Similar dissolution profiles for Co have been reported before.[60]

Once the upper potential limit (UPL) is increased to 1.2 and 1.4 V_{RHE} (Figure 5b and c), more Pt-oxide is formed/reduced and an additional peak due to the dissolution of less-noble-metal becomes more clearly resolved (peak 4, Figure 5b and c; $Co_{cathodic}$). Once again this is a consequence of the reduction of

DOI: 10.1021/acsaem.8b02142
ACS Appl. Energy Mater. 2019, 2, 3131−3141

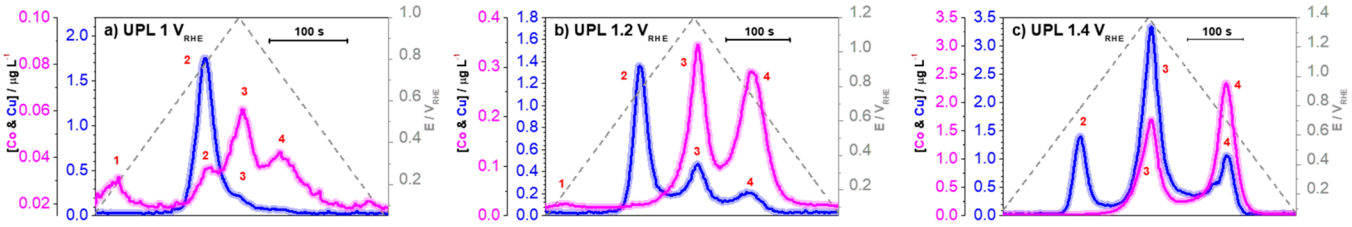

Figure 6. (a–c) EFC-ICP-MS measurements comparison of Cu and Co dissolution profiles for our in-house designed Pt–Cu/C electrocatalyst and the commercial Pt–Co/C electrocatalyst after PCA during slow cycles (0.1 M $HClO_4$, 5 mV s^{-1}, 0.05–1.*X* V_{RHE}, *X* = 0, 2, and 4). Peak 1 corresponds to OPD species, peak 2 to UPD species, while peaks 3 and 4 correspond to anodic and cathodic corrosion of Cu and Co, respectively. Each metal has its own *Y* axis to better compare the profiles despite the detected concentration differences.

Pt-oxide triggering a subsequent removal of the less-noble-metal in the process.[26,44,45] On the other hand, Co_{UPD} coverage is highly insignificant. In fact it could not be associated with any detectable dissolution peak in our investigation. This points out that more or less the entire amount of anodically and cathodically dissolved Co was flushed away from the active surface in the present flow-based system (EFC-ICP-MS) and does not redeposit or interact with the Pt surface in any significant way. As in the case of Pt–Cu/C electrocatalysts, we notice that the maxima of peak 3-Co_{anodic} and peak 3′-Pt_{anodic} are aligned, while the onset of peak 4-$Co_{cathodic}$ occurs after the onset of peak 4′-$Pt_{cathodic}$.[26,44,45] Thus, the Pt-M interaction is significantly different in the case of Pt–Co/C electrocatalysts than in the Pt–Cu/C counterpart. By contrast, the behavior of dealloying (in other words, removal of the less-noble-metal from the crystal structure in the form of cathodic and anodic dissolution) is very similar for both alloy systems and for both components (Pt and M).

It needs to be stressed again that the same trend is not directly applicable to PEMFC since in this report we used a flow system and thus the Pt surface|polymer(Nafion)|liquid interface. We presume that in a real application, any effects due to Co dissolution would be (much) more severe (e.g., due to unwanted Fenton reactions[61]). Thus, there is a high need for further development of ex situ chemical activation processes by the producers, where EFC-ICP-MS can act as a tool for detection of less-noble-metal "leakage".

Comparison of Cu and Co Dissolution from Pt–Cu/C and Pt–Co/C Electrocatalysts Based on the Results of EFC-ICP-MS. Plotting dissolution profiles for Cu and Co on the same graph (see also Figure S12c for comparison of both less-noble-metal dissolutions during PCA) shows that both metals behave completely differently already at lowest UPL of 1.0 V_{RHE} (Figure 6a). As mentioned above, the main difference can be ascribed to the thermodynamic interaction, that is, the Pt-M interaction (M_{UPD}, peak 2). Briefly, in the case of Pt surface|polymer(Nafion)|liquid setup the Pt–Cu/C electrocatalyst seems to have a much higher coverage of Cu_{UPD}, which gets stripped upon the anodic scan. On the other hand, the Pt–Co/C electrocatalyst material should not suffer from the same issue. Interestingly, in this work, certain amount of Co_{UPD} has been detected which means that the interaction is present at least to some extent, however not to the point of affecting the ORR performance (Figure 2d and e).

Upon raising the UPL to 1.2 or 1.4 V_{RHE} a difference in detected M_{UPD} species is noticed (Figure 6b and c, peak 2). In the case of Pt–Cu/C electrocatalyst, peak 2 (Cu_{UPD}) remains the dominant dissolution process to 1.4 V_{RHE}. Furthermore, in the case of Pt–Co/C electrocatalyst, $Co_{cathodic}$ has a higher contribution to the overall dissolution than Co_{anodic}, while the actual contributions in the case of our Pt–Cu/C electrocatalyst are masked by the Pt–Cu interaction (Cu_{UPD}). From deconvolution of UPD dissolution peaks (peak 2) and subsequent calculation, a surface coverage of Pt surface with Cu or Co can be obtained (see also Figure S13). In this way, an intrinsic interaction of dissolved less-noble-metals with Pt surface can be estimated. From the coverages presented in Figure 7, it is clear that Co is covering orders of magnitude

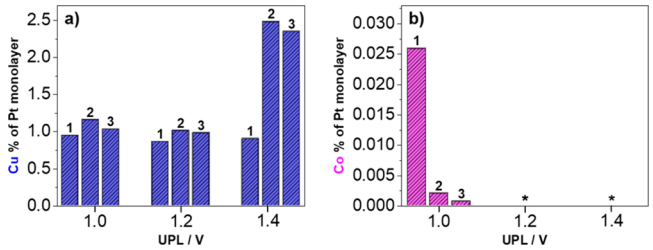

Figure 7. Percentage of Pt monolayer coverage as a consequence of varying the UPL during slow potentiodynamic treatment (from 0.05 to 1.*X* V_{RHE}, *X* = 0, 2, and 4, 5 mV s^{-1}) in the case of (a) Pt–Cu/C electrocatalyst and (b) Pt–Co/C electrocatalyst measured after PCA. 1, 2, and 3 represent each of the three slow cycles for each UPL (*the contribution of the UPD peak for Pt–Co/C electrocatalyst was too small for deconvolution and subsequent calculation). An example of UPD peak deconvolution and subsequent calculation can be found in Figure S13.

smaller portion of Pt surface compared to Cu. These very low coverages indicate that Co ions are more effectively washed out of the electrocatalyst compared to the Cu ions. Most likely, this is due to the fact that Cu is stabilized via thermodynamic deposition involving UPD monolayer coverage at the Pt surface up to the potential of 0.84 V_{RHE} and as OPD below 0.34 V_{RHE}.[21] If we compare potential limits within which each metal is stable (from 0.05 to 1.*X* V_{RHE}, *X* = 0, 2, and 4) and estimate the time available for the metal to be washed away, it is straightforward to realize that Cu remains "trapped" longer compared to Co, which is only stable below 0.6 V_{RHE} and can only form up to 60% of a monolayer,[58] compared to Cu that is stable at the very least up to 0.84 V_{RHE}.[21] Therefore, one can use the present qualitative evaluation of conditions (potential windows) within which the less-noble-metals are stable or unstable. This has important implications for understanding the effect of dealloyed less-noble-metal on ORR occurring in PEMFC. The full effect of surface Pt-M interactions on specific activity measured with TF-RDE, however, does not completely reveal the issues present in the real application due to the different behavior of inner and outer Helmholtz plane in the case of Pt surface|polymer(Nafion)|liquid interface in contrast to the Pt surface|polymer(Nafion)|gas phase interface.[19]

DOI: 10.1021/acsaem.8b02142
ACS Appl. Energy Mater. 2019, 2, 3131–3141

Furthermore, the diffusion-limiting currents in the TF-RDE setup are usually reached already at 0.8 V_{RHE}. This prevents a direct comparison with PEMFCs where high current densities are observed at lower potentials, for example, 0.6 V_{RHE}. At such conditions, the kinetic ORR currents would most likely be affected. Much work is still needed to answer the intriguing question proposed recently by Stephens et al.,[62] namely, if the spectacular RDE-measured activities at 0.9 V_{RHE} for Pt and Pt-alloys[4,6−8,63] can indeed be translated to the technological application at higher current densities (above 1 A cm^{-2}) and high overpotentials (below 0.8 V_{RHE}).[62] The present study speculates that surface blocking of the dealloying/leaching less-noble-metal is one of the main issues that needs to be addressed along these lines.

CONCLUSIONS

Using a complementary analytical approach involving the highly sensitive EFC-ICP-MS tool, we compared the detailed dissolution behavior of two Pt-alloy systems—a commercial Pt−Co/C electrocatalyst and our in-house designed Pt−Cu/C electrocatalyst. The main conclusions are as follows: (i) Both electrocatalysts lose significant amounts of their less-noble-metal component (Co or Cu) during the electrochemical activation protocol. While this was fully expected for the "as prepared" Pt−Cu/C electrocatalyst, the result is rather surprising for the "as received" Pt−Co/C electrocatalyst which had already been ex situ activated by the producer. (ii) In the case of Pt−Cu/C electrocatalyst, potential-hold-activated electrocatalyst leaks about an order of magnitude more less-noble-metal during each cycle in contrast to the potential-cycling-activated electrocatalyst. Locally, this can lead to high enough less-noble-metal concentrations to affect the corresponding electrochemical reactions - due to either noncovalent or thermodynamic (UPD) interactions. (iii) In the case of Pt−Cu/C electrocatalyst, the degree of less-noble-metal leakage influences ORR because of the Pt-M (UPD) interaction. This interaction is far more detrimental for the Pt−Cu/C electrocatalyst, where Cu_{UPD} has a significant contribution to the overall dissolution profile of Cu (as detected using EFC-ICP-MS). However, once adequately activated, our in-house designed Pt−Cu/C electrocatalyst exhibited a notably higher (200%) specific activity at 0.9 V_{RHE} than the Pt−Co/C electrocatalyst in TF-RDE setup. This demonstrates that ORR and ESA are independent of the employed activation protocol (PHA or PCA). (iv) Therefore, the main difference in dissolution behavior between both electrocatalysts lies in the Pt−M (UPD) interaction, while the anodic and cathodic corrosion properties (dealloying) of both systems are comparable. We argue that such a behavior could be extended to other binary Pt-alloy nanoparticulate electrocatalyst, regardless of their particle size, morphology, chemical composition, and alloying (less-noble) element. Such a generalization will be investigated in the near future. (v) While the present findings provide evidence about much different behavior of both Pt-alloy electrocatalysts studied at the Pt surfacelpolymer(Nafion)lliquid interface, the rather strong dissolution of any less-noble-metal at Pt surfacel polymer(Nafion)lgas interface should be prevented prior to implementation in MEA (also due to the possible unwanted Fenton reaction in the proton exchange membrane[61]). For that, new strategies for ex situ activation[64] are needed that take into the consideration not only anodic and cathodic corrosion of the less-noble-metal but also the noncovalent and Pt-M (UPD) interactions for each Pt-M system individually. In this sense EFC-ICP-MS as a complementary characterization tool to TF-RDE could play a vital role in determination of the degree of less-noble-metal leaking and thus the success of a particular ex situ activation protocol.

ASSOCIATED CONTENT

Supporting Information

The Supporting Information is available free of charge on the ACS Publications website at DOI: 10.1021/acsaem.8b02142.

Scheme of EFC setup, EFC-ICP-MS, TEM, and electrochemical TF-RDE measurements (PDF)

AUTHOR INFORMATION

Corresponding Authors

*E-mail: primoz.jovanovic@ki.si.
*E-mail: miran.gaberscek@ki.si.

ORCID

Matija Gatalo: 0000-0002-5041-7280
Primož Jovanovič: 0000-0003-2477-3895
Martin Šala: 0000-0001-7845-860X
Vid Simon Šelih: 0000-0002-2433-5249
Nejc Hodnik: 0000-0002-7113-9769
Miran Gaberščček: 0000-0002-8104-1693

Notes

The authors declare no competing financial interest.

ACKNOWLEDGMENTS

Authors gratefully acknowledge the financial support of the Slovenian Research Agency (ARRS) through the Research Core Funding Programme P2-0152 and P2-0393 and Projects Z2-8161 and Z1-9165. Part of the work was carried out within the NATO Science for Peace Project EAP.SFPP 984925—"DURAPEM".

REFERENCES

(1) Gröger, O.; Gasteiger, H. A.; Suchsland, J.-P. Review—Electromobility: Batteries or Fuel Cells? *J. Electrochem. Soc.* **2015**, *162*, 2605−2622.
(2) Marković, N. M. Electrocatalysis: Interfacing Electrochemistry. *Nat. Mater.* **2013**, *12*, 101−102.
(3) U.S. Department of Energy. *Fuel Cell Technologies Market Report (2014)*; 2013.
(4) Stamenković, V. R.; Fowler, B.; Mun, B. S.; Wang, G.; Ross, P. N.; Lucas, C. a; Marković, N. M. Improved Oxygen Reduction Activity on Pt3Ni(111) via Increased Surface Site Availability. *Science* **2007**, *315*, 493−497.
(5) Strasser, P.; Koh, S.; Anniyev, T.; Greeley, J.; More, K.; Yu, C.; Liu, Z.; Kaya, S.; Nordlund, D.; Ogasawara, H.; Toney, M. F.; Nilsson, A. Lattice-Strain Control of the Activity in Dealloyed Core-Shell Fuel Cell Catalysts. *Nat. Chem.* **2010**, *2*, 454−460.
(6) Huang, X.; Zhao, Z.; Cao, L.; Chen, Y.; Zhu, E.; Lin, Z.; Li, M.; Yan, A.; Zettl, A.; Wang, Y. M.; Duan, X.; Mueller, T.; Huang, Y. High-Performance Transition Metal-Doped Pt3Ni Octahedra for Oxygen Reduction Reaction. *Science* **2015**, *348*, 1230−1234.
(7) Chen, C.; Kang, Y.; Huo, Z.; Zhu, Z.; Huang, W.; Xin, H. L.; Snyder, J. D.; Li, D.; Herron, J. A.; Mavrikakis, M.; Chi, M.; More, K. L.; Li, Y.; Markovic, N. M.; Somorjai, G. A.; Yang, P.; Stamenkovic, V. R. Highly Crystalline Multimetallic Nanoframes with Three-Dimensional Electrocatalytic Surfaces. *Science* **2014**, *343*, 1339−1343.
(8) Bu, L.; Zhang, N.; Guo, S.; Zhang, X.; Li, J.; Yao, J.; Wu, T.; Lu, G.; Ma, J.-Y.; Su, D.; Huang, X. Biaxially Strained PtPb/Pt Core/shell

DOI: 10.1021/acsaem.8b02142
ACS Appl. Energy Mater. 2019, 2, 3131−3141

Nanoplate Boosts Oxygen Reduction Catalysis. *Science* **2016**, *354*, 1410−1414.
(9) Pourbaix, M.. *Atlas of Electrochemical Equilibria in Aqueous Solutions*, 2nd ed.; National Association of Corrosion: Houston, TX, 1974.
(10) Gasteiger, H. A.; Kocha, S. S.; Sompalli, B.; Wagner, F. T. Activity Benchmarks and Requirements for Pt, Pt-Alloy, and Non-Pt Oxygen Reduction Catalysts for PEMFCs. *Appl. Catal., B* **2005**, *56*, 9−35.
(11) Mayrhofer, K. J. J.; Juhart, V.; Hartl, K.; Hanzlik, M.; Arenz, M. Adsorbate-Induced Surface Segregation for Core-Shell Nanocatalysts. *Angew. Chem., Int. Ed.* **2009**, *48*, 3529−3531.
(12) Jovanovič, P.; Šelih, V. S.; Šala, M.; Hočevar, S. B.; Pavlišič, A.; Gatalo, M.; Bele, M.; Ruiz-Zepeda, F.; Čekada, M.; Hodnik, N.; Gaberšček, M. Electrochemical in-Situ Dissolution Study of Structurally Ordered, Disordered and Gold Doped PtCu3 Nanoparticles on Carbon Composites. *J. Power Sources* **2016**, *327*, 675−680.
(13) Hodnik, N.; Jeyabharathi, C.; Meier, J. C.; Kostka, A.; Phani, K. L.; Rečnik, A.; Bele, M.; Hočevar, S.; Gaberšček, M.; Mayrhofer, K. J. J. Effect of Ordering of PtCu3 Nanoparticle Structure on the Activity and Stability for the Oxygen Reduction Reaction. *Phys. Chem. Chem. Phys.* **2014**, *16*, 13610−13615.
(14) Yu, Z.; Zhang, J.; Liu, Z.; Ziegelbauer, J. M.; Xin, H.; Dutta, I.; Muller, D. A.; Wagner, F. T. Comparison between Dealloyed PtCo3 and PtCu3 Cathode Catalysts for Proton Exchange Membrane Fuel Cells. *J. Phys. Chem. C* **2012**, *116*, 19877−19885.
(15) Stephens, I. E. L.; Bondarenko, A. S.; Perez-Alonso, F. J.; Calle-Vallejo, F.; Bech, L.; Johansson, T. P.; Jepsen, A. K.; Frydendal, R.; Knudsen, B. P.; Rossmeisl, J.; Chorkendorff, I. Tuning the Activity of Pt(111) for Oxygen Electroreduction by Subsurface Alloying. *J. Am. Chem. Soc.* **2011**, *133*, 5485−5491.
(16) Seh, Z. W.; Kibsgaard, J.; Dickens, C. F.; Chorkendorff, I.; Nørskov, J. K.; Jaramillo, T. F. Combining Theory and Experiment in Electrocatalysis: Insights into Materials Design. *Science* **2017**, *355*, No. eaad4998.
(17) Tindall, G. W.; Cadle, S. H.; Bruckenstein, S. Inhibition of the Reduction of Oxygen at a Platinum Electrode by the Deposition of a Monolayer of Copper at Underpotential. *J. Am. Chem. Soc.* **1969**, *91*, 2119−2120.
(18) Kokkinidis, G.; Jannakoudakis, D. Oxygen Reduction on Pt and Cu Surfaces Modified by Underpotential Adsorbates. *J. Electroanal. Chem. Interfacial Electrochem.* **1984**, *162*, 163−173.
(19) Durst, J.; Chatenet, M.; Maillard, F. Impact of Metal Cations on the Electrocatalytic Properties of Pt/C Nanoparticles at Multiple Phase Interfaces. *Phys. Chem. Chem. Phys.* **2012**, *14*, 13000−13009.
(20) Strmcnik, D.; Kodama, K.; Van Der Vliet, D.; Greeley, J.; Stamenkovic, V. R.; Marković, N. M. The Role of Non-Covalent Interactions in Electrocatalytic Fuel-Cell Reactions on Platinum. *Nat. Chem.* **2009**, *1*, 466−472.
(21) Jia, Q.; Ramaker, D. E.; Ziegelbauer, J. M.; Ramaswamy, N.; Halder, A.; Mukerjee, S. Fundamental Aspects of Ad-Metal Dissolution and Contamination in Low and Medium Temperature Fuel Cell Electrocatalysis: A Cu Based Case Study Using In Situ Electrochemical X-Ray Absorption Spectroscopy. *J. Phys. Chem. C* **2013**, *117*, 4585−4596.
(22) Markovic, N.; Ross, P. N. Effect of Anions on the Underpotential Deposition of Copper on Platinum (111) and Platinum (100) Surfaces. *Langmuir* **1993**, *9*, 580−590.
(23) Herrero, E.; Buller, L. J.; Abruña, H. D. Underpotential Deposition at Single Crystal Surfaces of Au, Pt, Ag and Other Materials. *Chem. Rev.* **2001**, *101*, 1897−1930.
(24) McBreen, J. EXAFS Studies of Adsorbed Copper on Carbon-Supported Platinum. *J. Electroanal. Chem.* **1993**, *357*, 373−386.
(25) Jovanovič, P.; Selih, V. S.; Šala, M.; Hočevar, S.; Ruiz-Zepeda, F.; Hodnik, N.; Bele, M.; Gaberšček, M. Potentiodynamic Dissolution Study of PtRu/C Electrocatalyst in the Presence of Methanol. *Electrochim. Acta* **2016**, *211*, 851−859.
(26) Jovanovič, P.; Pavlišič, A.; Šelih, V. S.; Šala, M.; Bele, M.; Hodnik, N.; Hočevar, S.; Gaberšček, M. New Insight into Platinum Dissolution from Nanoparticulate Platinum-Based Electrocatalysts Using Highly Sensitive In Situ Concentration Measurements. *ChemCatChem* **2014**, *6*, 449−453.
(27) Jovanovič, P.; Hodnik, N.; Ruiz-Zepeda, F.; Arčon, I.; Jozinović, B.; Zorko, M.; Bele, M.; Šala, M.; Šelih, V. S.; Hočevar, S.; Gaberšček, M. Electrochemical Dissolution of Iridium and Iridium Oxide Particles in Acidic Media: Transmission Electron Microscopy, Electrochemical Flow Cell Coupled to Inductively Coupled Plasma Mass Spectrometry and X-Ray Absorption Spectros-Copy Study. *J. Am. Chem. Soc.* **2017**, *139*, 12837−12846.
(28) Hodnik, N.; Jovanovič, P.; Pavlišič, A.; Jozinović, B.; Zorko, M.; Bele, M.; Šelih, V. S.; Šala, M.; Hočevar, S.; Gaberšček, M. New Insights into Corrosion of Ruthenium and Ruthenium Oxide Nanoparticles in Acidic Media. *J. Phys. Chem. C* **2015**, *119*, 10140−10147.
(29) Bele, M.; Gaberčšk, M.; Kapun, G.; Hodnik, N.; Hočevar, S. Electrocatalytic Composite(s), Associated Composition(s), and Associated Process(es). U.S. Patent US9147885 (B2), 2015; Japanese Patent JP6028027 (B2), 2016; European Patent EP2735044 (A2), 2014; Int. Patent WO2013012398 (A2), 2013.
(30) Bele, M.; Jovanovič, P.; Pavlišič, A.; Jozinović, B.; Zorko, M.; Rečnik, A.; Chernyshova, E.; Hočevar, S.; Hodnik, N.; Gaberšček, M. A Highly Active PtCu3 Intermetallic Core-Shell, Multilayered Pt-Skin, Carbon Embedded Electrocatalyst Produced by a Scale-up Sol−Gel Synthesis. *Chem. Commun.* **2014**, *50*, 13124−13126.
(31) Hodnik, N.; Bele, M.; Hočevar, S. New Pt-Skin Electrocatalysts for Oxygen Reduction and Methanol Oxidation Reactions. *Electrochem. Commun.* **2012**, *23*, 125−128.
(32) Mayrhofer, K. J. J.; Strmcnik, D.; Blizanac, B. B.; Stamenkovic, V.; Arenz, M.; Markovic, N. M. Measurement of Oxygen Reduction Activities via the Rotating Disc Electrode Method: From Pt Model Surfaces to Carbon-Supported High Surface Area Catalysts. *Electrochim. Acta* **2008**, *53*, 3181−3188.
(33) van der Vliet, D.; Strmčnik, D.; Wang, C.; Stamenković, V. R.; Marković, N. M.; Koper, M. T. M. On the Importance of Correcting for the Uncompensated Ohmic Resistance in Model Experiments of the Oxygen Reduction Reaction. *J. Electroanal. Chem.* **2010**, *647*, 29−34.
(34) Wang, D.; Xin, H. L.; Hovden, R.; Wang, H.; Yu, Y.; Muller, D. A.; DiSalvo, F. J.; Abruña, H. D. Structurally Ordered Intermetallic Platinum-Cobalt Core-Shell Nanoparticles with Enhanced Activity and Stability as Oxygen Reduction Electrocatalysts. *Nat. Mater.* **2013**, *12*, 81−87.
(35) Hodnik, N.; Jeyabharathi, C.; Meier, J. C.; Kostka, A.; Phani, K. L.; Rečnik, A.; Bele, M.; Hočevar, S.; Gaberšček, M.; Mayrhofer, K. J. J. Effect of Ordering of $PtCu_3$ Nanoparticle Structure on the Activity and Stability for the Oxygen Reduction Reaction. *Phys. Chem. Chem. Phys.* **2014**, *16*, 13610−13615.
(36) Koh, S.; Toney, M. F.; Strasser, P. Activity-Stability Relationships of Ordered and Disordered Alloy Phases of Pt_3Co Electrocatalysts for the Oxygen Reduction Reaction (ORR). *Electrochim. Acta* **2007**, *52*, 2765−2774.
(37) Matsutani, K.; Hayakawa, K.; Tada, T. Effect of Particle Size of Platinum and Platinum-Cobalt Catalysts on Stability Against Load Cycling. *Platinum Met. Rev.* **2010**, *54*, 223−232.
(38) Castanheira, L.; Silva, W. O.; Lima, F. H. B.; Crisci, A.; Dubau, L.; Maillard, F. Carbon Corrosion in Proton-Exchange Membrane Fuel Cells: Effect of the Carbon Structure, the Degradation Protocol, and the Gas Atmosphere. *ACS Catal.* **2015**, *5*, 2184−2194.
(39) Castanheira, L.; Dubau, L.; Mermoux, M.; Berthomé, G.; Caqué, N.; Rossinot, E.; Chatenet, M.; Maillard, F. Carbon Corrosion in Proton-Exchange Membrane Fuel Cells: From Model Experiments to Real-Life Operation in Membrane Electrode Assemblies. *ACS Catal.* **2014**, *4*, 2258−2267.
(40) Bele, M.; Jovanovič, P.; Pavlišič, A.; Jozinović, B.; Zorko, M.; Rečnik, A.; Chernyshova, E.; Hočevar, S.; Hodnik, N.; Gaberšček, M. A. *Chem. Commun.* **2014**, *50*, 13124−13126.

DOI: 10.1021/acsaem.8b02142
ACS Appl. Energy Mater. 2019, 2, 3131−3141

(41) Arenz, M.; Mayrhofer, K. J. J.; Stamenkovic, V.; Blizanac, B. B.; Tomoyuki, T.; Ross, P. N.; Markovic, N. M. The Effect of the Particle Size on the Kinetics of CO Electrooxidation on High Surface Area Pt Catalysts. *J. Am. Chem. Soc.* **2005**, *127*, 6819−6829.
(42) Cadle, S. H.; Bruckenstein, S. Inhibition of Hydrogen Absorption by Submonolayer Deposition of Metals on Platinum. *Anal. Chem.* **1971**, *43*, 1858−1862.
(43) Leung, L. W. H.; Gregg, T. W.; Goodman, D. W. Electrochemical and Ultrahigh Vacuum Characterization of Ultrathin Copper Films on platinum(111). *Langmuir* **1991**, *7*, 3205−3210.
(44) Topalov, A. A.; Cherevko, S.; Zeradjanin, A. R.; Meier, J. C.; Katsounaros, I.; Mayrhofer, K. J. J. Towards a Comprehensive Understanding of Platinum Dissolution in Acidic Media. *Chem. Sci.* **2014**, *5*, 631−638.
(45) Topalov, A. A.; Katsounaros, I.; Auinger, M.; Cherevko, S.; Meier, J. C.; Klemm, S. O.; Mayrhofer, K. J. J. Dissolution of Platinum: Limits for the Deployment of Electrochemical Energy Conversion? *Angew. Chem., Int. Ed.* **2012**, *51*, 12613−12615.
(46) Čolić, V.; Bandarenka, A. S. Pt Alloy Electrocatalysts for the Oxygen Reduction Reaction: From Model Surfaces to Nanostructured Systems. *ACS Catal.* **2016**, *6*, 5378−5385.
(47) Mani, P.; Srivastava, R.; Strasser, P. Dealloyed Pt-Cu Core-Shell Nanoparticle Electrocatalysts for Use in PEM Fuel Cell Cathodes. *J. Phys. Chem. C* **2008**, *112*, 2770−2778.
(48) Wang, D.; Yu, Y.; Xin, H. L.; Hovden, R.; Ercius, P.; Mundy, J. A.; Chen, H.; Richard, J. H.; Muller, D. A.; DiSalvo, F. J.; Abruña, H. D. Tuning Oxygen Reduction Reaction Activity via Controllable Dealloying: A Model Study of Ordered Cu_3Pt/C Intermetallic Nanocatalysts. *Nano Lett.* **2012**, *12*, 5230−5238.
(49) Wang, D.; Yu, Y.; Zhu, J.; Liu, S.; Muller, D. a; Abruña, H. D. Morphology and Activity Tuning of Cu_3Pt/C Ordered Intermetallic Nanoparticles by Selective Electrochemical Dealloying. *Nano Lett.* **2015**, *15*, 1343−1348.
(50) Oezaslan, M.; Hasché, F.; Strasser, P. $PtCu_3$, PtCu and Pt_3Cu Alloy Nanoparticle Electrocatalysts for Oxygen Reduction Reaction in Alkaline and Acidic Media. *J. Electrochem. Soc.* **2012**, *159*, 444−454.
(51) Gatalo, M.; Jovanovič, P.; Polymeros, G.; Grote, J. P.; Pavlišič, A.; Ruiz-Zepeda, F.; Šelih, V. S.; Šala, M.; Hočevar, S.; Bele, M.; Mayrhofer, K. J. J.; Hodnik, N.; Gaberšček, M. Positive Effect of Surface Doping with Au on the Stability of Pt-Based Electrocatalysts. *ACS Catal.* **2016**, *6*, 1630−1634.
(52) Gatalo, M.; Jovanovič, P.; Ruiz-Zepeda, F.; Pavlišič, A.; Robba, A.; Bale, M.; Dražić, G.; Gaberšček, M.; Hodnik, N. Insights into Electrochemical Dealloying of Cu out of Au-Doped Pt-Alloy Nanoparticles at the Sub-Nano-Scale. *J. Electrochem. Sci. Eng.* **2018**, *8*, 87−100.
(53) Ruiz-Zepeda, F.; Gatalo, M.; Jovanovič, P.; Pavlišič, A.; Bele, M.; Hodnik, N.; Gaberšček, M. Gold Doping in $PtCu_3$/HSAC Nanoparticles and Their Morphological, Structural, and Compositional Changes during Oxygen Reduction Reaction Electrochemical Cycling. *ChemCatChem* **2017**, *9*, 3904−3911.
(54) Jia, F.; Guo, L.; Liu, H. Mitigation Strategies for Hydrogen Starvation under Dynamic Loading in Proton Exchange Membrane Fuel Cells. *Energy Convers. Manage.* **2017**, *139*, 175−181.
(55) Bona, D.; Curtin, D. E.; Pedrazzo, F.; Tresso, E. M. Using a Stack Shunt to Mitigate Catalyst Support Carbon Corrosion in Polymer Electrolyte Membrane Fuel Cell Stacks During Start-Stop Cycling. *J. Fuel Cell Sci. Technol.* **2014**, *11*, 011010.
(56) Meier, J. C.; Galeano, C.; Katsounaros, I.; Topalov, A. a.; Kostka, A.; Schüth, F.; Mayrhofer, K. J. J. Degradation Mechanisms of Pt/C Fuel Cell Catalysts under Simulated Start-Stop Conditions. *ACS Catal.* **2012**, *2*, 832−843.
(57) Gu, W.; Carter, R. N.; Yu, P. T.; Gasteiger, H. A. Start/Stop and Local H_2 Starvation Mechanisms of Carbon Corrosion: Model vs. Experiment; *ECS* **2007**, *11*, 963−973.
(58) Herrero, E.; Li, J.; Abruña, H. D. Electrochemical, in-Situ Surface EXAFS and CTR Studies of Co Monolayers Irreversibly Adsorbed onto Pt(111). *Electrochim. Acta* **1999**, *44*, 2385−2396.
(59) Mendoza-Huizar, L. H.; Rios-Reyes, C. H. Underpotential Deposition of Cobalt onto Polycrystalline Platinum. *J. Solid State Electrochem.* **2011**, *15*, 737−745.
(60) Ahluwalia, R. K.; Papadias, D. D.; Kariuki, N. N.; Peng, J.-K.; Wang, X.; Tsai, Y.; Graczyk, D. G.; Myers, D. J. Potential Dependence of Pt and Co Dissolution from Platinum-Cobalt Alloy PEFC Catalysts Using Time-Resolved Measurements. *J. Electrochem. Soc.* **2018**, *165*, 3024−3035.
(61) Strlič, M.; Kolar, J.; Šlih, V.-S.; Kočar, D.; Pihlar, B. A comparative study of several transition metals in Fenton-like reaction system at circum-neutral pH. *Acta Chim. Slov.* **2003**, *50*, 619−632.
(62) Stephens, I. E. L.; Rossmeisl, J.; Chorkendorff, I. Toward Sustainable Fuel Cells. *Science* **2016**, *354*, 1378−1379.
(63) Li, M.; Zhao, Z.; Cheng, T.; Fortunelli, A.; Chen, C.-Y.; Yu, R.; Zhang, Q.; Gu, L.; Merinov, B.; Lin, Z.; Zhu, E.; Yu, T.; Jia, Q.; Guo, J.; Zhang, L.; Goddard, W. A.; Huang, Y.; Duan, X. Ultrafine Jagged Platinum Nanowires Enable Ultrahigh Mass Activity for the Oxygen Reduction Reaction. *Science* **2016**, *354*, 1414−1419.
(64) Gatalo, M.; Moriau, L.; Petek, U.; Ruiz-Zepeda, F.; Šala, M.; Grom, M.; Galun, T.; Jovanovič, P.; Pavlišič, A.; Bele, M.; Hodnik, N.; Gaberšček, M. CO-Assisted Ex-Situ Chemical Activation of Pt-Cu/C Oxygen Reduction Reaction Electrocatalyst. *Electrochim. Acta* **2019**, *306*, 377−386.

DOI: 10.1021/acsaem.8b02142
ACS Appl. Energy Mater. 2019, 2, 3131−3141